IGBT FINITE ELEMENT MODEL FOR FIBRE BRAGG GRATING SENSOR INSTALLATION ANALYSIS

IGBT FINITE ELEMENT MODEL FOR FIBRE BRAGG GRATING SENSOR INSTALLATION ANALYSIS

Damian S Vilchis-Rodriguez[1], Shiying Chen[1], Siniša Djurović[1*], Mike Barnes[1], Paul McKeever[2], Chunjiang Jia[2]

[1]Deparment of Electrical and Electronic Engineering, The University of Manchester, Manchester, UK
[2]Offshore Renewable Energy (ORE) Catapult, Blyth, UK
**Damian.Vilchis-Rodriguez@manchester.ac.uk*

Keywords: IGBT, junction temperature, finite element, thermal analysis, Fibre Bragg Grating

Abstract

An IGBT finite element model aimed at facilitating the assessment of Fibre Bragg Grating sensing based direct on-chip temperature monitoring is first presented in this paper. A commercial off-the-shelf IGBT module geometry is characterised, and a thermo-electrical finite element model is then established using its features. The model is subsequently employed to evaluate the local thermal disturbances that may be introduced by the installation of the optical based temperature sensor directly on the top surface of the IGBT chip. The effects of the sensor thermal interface material characteristics, e.g., thermal conductivity and size, in the local temperature environment are investigated.

1 Introduction

The Insulated Gate Bipolar Transistor (IGBT) is at the core of a myriad of power electronics interfacing devices and power electronics applications, ranging from MW size high voltage direct current links, wind power generators to electric car inverters [1]. Owing to temperature fluctuations that occur inside an IGBT package during operation, mechanical stress is produced on the joint surfaces between layers during thermal expansion and contraction. This stress can be further exaggerated by the large coefficient of thermal expansion (CTE) disparities that typically exist between the adjacent layers [2]. The resulting cumulative mechanical stress between adjacent layers causes changes in the joint structure (ageing), leading eventually to failure of the IGBT power module. The junction temperature fluctuation is considered as one of the main reasons for the device ageing [2]-[4]. Therefore, junction temperature is a parameter commonly used to assess the device operating condition and predict its remaining useful life [5]-[6].

IGBT modules usually operate under severe space constraints in EMI rich environments. Fibre Bragg Grating (FBG) optical sensors are immune to electromagnetic interference, power passive, of small size and can be multiplexed and can be therefore considered a fitting technology for the direct measurement of IGBT junction temperature [7, 8]. However, for the effective heat transfer from the sensed surface to the sensor, a thermal interface material (TIM), with a suitable thermal conductivity is required. The fibre/TIM arrangement has the potential to disturb the original thermal environment where it is seated, biasing the measured temperature values. FBG sensing has a promising potential to unlock advanced direct thermal monitoring schemes in power electronic modules, however its application features, including the assessment of the influence on the inherent thermal conditions of the power modules have received limited attention. Direct measuring of electro-mechanical-thermal effects on the IGBT is extremely difficult, and such analysis are often conducted with the help of numerical models. For its capability to simulate the complex interactions between the different IGBT components and materials, the use of finite element (FE) models is commonly used in the detailed analysis of IGBTs thermal behaviour [9, 10].

In this paper a commercially available IGBT power module geometry is fully characterized, and a 3D electro-thermal FE model constructed. With the help of this model, the electrical and thermal disturbances that the installation of an optical sensor on the IGBT surface may introduce are investigated to assess the practicality FBG based direct IGBT junction temperature sensing, in an effort to shed further insight into the potential of this monitoring technology.

2 Module characterization

To analyse the sensor-IGBT thermal interaction, a FE model of a Semikron SKM50GB12T4 IGBT module is built using the Comsol 5.4 Multiphysics FE software. The FE model considers the simultaneous solution of thermal and electrical current equations. To build the FE model, the geometry of the physical IGBT module (Fig. 1), is fully characterized. Then, the FE model geometry is built based on the module dimensions and constitutive materials physical properties. For IGBT module geometry characterization, reference vertical and horizontal dimensions (baseplate thickness and silicon die width) were manually measured using high precision digital callipers. Then, detailed high resolution digital images of the IGBT module were taken. These were used to calculate the relevant module dimensions employing an image processing software and using as base values the reference dimensions previously measured. Fig. 2 shows a detail of the measured cross-sectional view of the actual test module layers. Fig. 3. shows a comparison between the module real geometry and

the FE model, where excellent agreement between the real module and the FE geometry is demonstrated. The geometrical dimensions of the several IGBT components are listed in Table 1, while Fig. 4. shows a picture of the full IGBT FE module geometry.

The main objective of this work is to analyse the IGBT thermal environment. Hence, to reduce model complexity and decrease computing time, only the module's left half side is considered in simulation. It should be noted that using a single IGBT chip from the module is possible with the reference physical device. To further simplify the model the diode operation is neglected in this study. Thus, the diode is disconnected from the electrical circuit. This is achieved by removing the respective bond wires, reducing further the model complexity. For switching operation simulation, pulsed current is injected in the IGBT collector terminal, while the bridge connector (emitter terminal) is assumed to be grounded. Thus, the gate connection does not play any active role in the simulations, therefore removal of the related bond wire from the model is possible. The simplified geometry used in the simulations and the model electrical terminals are shown in Fig. 5. As can be deduced form Fig. 5, for the investigated device the collector is at the bottom of the IGBT die while the emitter is at the top. The physical properties of the module constitutive materials can vary substantially between manufacturers [9, 10]. For simplicity, the material physical properties were selected from a range of values available in the open literature. The selected values were chosen to mimic, as close as possible, the behaviour of the physical model reported in the manufacturer datasheet. Table 2 shows the selected values used for the different module components materials physical properties.

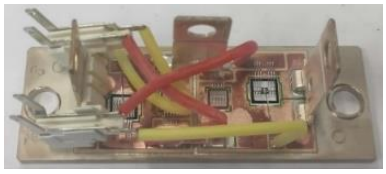

Fig. 1 Bare Semikron SKM50GB12T4 IGBT module

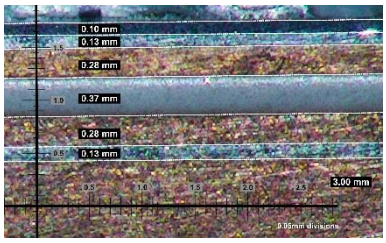

Fig. 2 IGBT module cross section, measurement detail

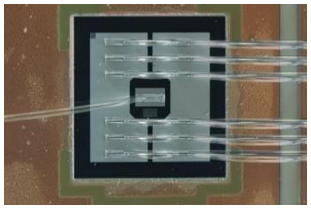

Fig. 3 Physical IGBT-FE model geometry comparison IGBT chip top view

Table 1 IGBT module dimensions

Layer name	Length [mm]	Width [mm]	Thickness [mm]	Diameter [mm]
Bond wire	-	-	-	0.25
Solder IGBT top	5.80	5.40	0.02	-
IGBT die	7.20	6.80	0.10	-
Solder IGBT bottom	7.40	7.00	0.13	-
Copper layer 1	-	-	0.28	-
Ceramic	30.50	28.00	0.37	-
Copper layer 2	28.50	26.00	0.28	-
Solder baseplate	28.50	26.00	0.13	-
Copper baseplate	91.00	31.00	3.00	-

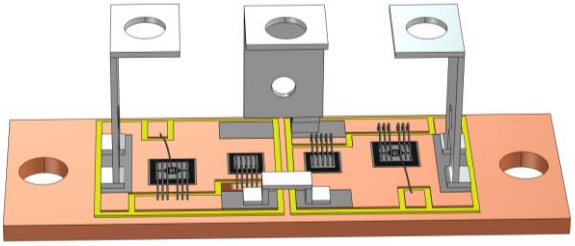

Fig. 4 FE module model geometry

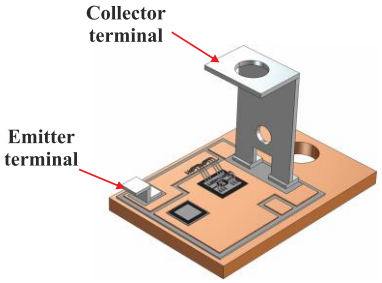

Fig. 5 Simplified FE model geometry

Table 2 IGBT materials physical properties

Layer type	Material	Thermal conductivity [W/m·K]	Heat capacity [J/(kg·K)]	Density [kg/m^3]	Electrical conductivity [S/m]
Bondwire	Al	240	930.6	2700	3.670e7
Solder	SnAgPb	63	232.0	7370	9.100e6
IGBT	Si	119	757.7	2329	$3.24e5 \times T^{-1.408}$
Copper	Cu	396	392.6	8850	5.998e7
Ceramic	Al_2O_3	25	880.0	3890	1.502e-7

Given that the IGBT die is responsible for most of the electrical conduction losses and can consequently be considered as the principal heat source of the module, a temperature dependent electrical conductivity characteristic [10] is adopted for this component, to achieve a more realistic simulation. The parameters values used for the IGBT conductivity equation were selected to follow an equivalent silicon electrical conductivity, derived by using the commercial IGBT module V_{CE}-I_C characteristic, the module geometric dimensions and the electrical conductivity of the IGBT materials listed in Table 2 that are part of the current conduction path [10].

3 Model implementation and simulation results

As mentioned in section 2, to simulate switching operation a pulsed current is injected to the model collector terminal. However, to avoid convergence problems during simulation, a trapezoidal waveform is adopted for the injected current, instead of a square one. A 50% duty cycle and rise and fall times of 1/100th of the switching period are considered in the simulations. Comsol's 'Heat transfer in solids' and 'Electric Currents' physics are used in the numerical simulation. A fully coupled, constant Newton solver is selected for the time-domain simulations with an intermediate, time stepping BDF method. Results from stationary studies are used to set the initial conditions for time-domain simulations.

In the commercial module, the components shown in Fig. 1 are encapsulated in silica gel and further protected by rigid plastic casing. Therefore, a low heat transfer value of 5 W/(m^2·K) typically used for natural convection cooled systems [11] is assumed for all the exposed module components' surfaces above the baseplate lowest plane. In contrast, a higher 2500 W/(m^2·K) heat transfer rate is considered for the baseplate bottom surface, to emulate a more robust forced cooling solution [11]. A 33°C ambient temperature is considered in the simulations and mechanical effects (e.g., thermal expansion phenomena) are neglected.

3.1 Stationary analysis

The IGBT response under stationary conditions is analysed in this section. In the stationary simulations it is assumed that an equivalent, RMS current flows through the module terminals. For the duty cycle, fall and rise times considered in this paper the current RMS value is calculated as $0.7118 \cdot I_{max}$. The resulting temperature distribution on the IGBT exhibits a radial symmetry, this is illustrated in Fig. 6 where a plan view of the IGBT die is shown for a 4kHz, 50A simulation. As can be seen in Fig. 6, for the investigated IGBT module the hottest region in the silicon die is located around the inner edge of the top solder layer. A considerable temperature difference between the silicon regions in direct contact and those with no contact with the top solder layer is observed: the temperature difference between the hottest and coolest areas of the silicon die is more than 18°C. Fig. 7 shows a cross sectional view of the IGBT central axis of symmetry. As shown in the figure, the hottest regions on the vertical direction coincide with the bond wires' contact point. Thus, if the IGBT hottest area is to be monitored, the sensor must be ideally placed along the IGBT central axis of symmetry, in the gap between the two bond wire arrays, as pointed in Fig. 8.

3.2 Time domain analysis

Fig. 9 shows the time domain signal for temperature variations on the selected sensing point for the top solder layer top surface, and the silicon die top and bottom surfaces, with the IGBT operating at 4kHz, 50A. The figure shows that the temperature measured in the solder layer is very similar to that on the silicon top surface, while a temperature difference of about 0.5°C exist between the top and bottom surfaces of the IGBT die. For the investigated device, the highest temperature was found to occur toward the top of the silicon die. Further tests, at different current levels and switching frequencies were conducted. For all the cases (omitted here for brevity), the temperature in the investigated x,y position of the top solder layer was found to closely follow that of top surface of the silicon die: such results imply that temperature measurement at the top solder layer can be considered as an adequate indicator of the IGBT die temperature.

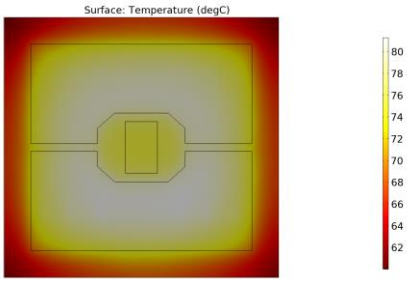

Fig. 6 FE silicon die stationary study temperature distribution results for a 50A Imax current

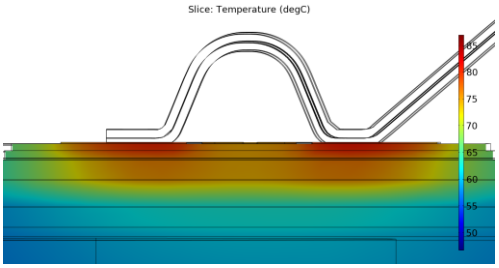

Fig. 7 IGBT temperature distribution, cross section view along the chip axis of symmetry

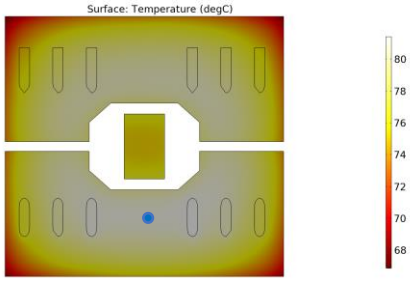

Fig. 8 Top solder layer temperature distribution with reference point marked in blue

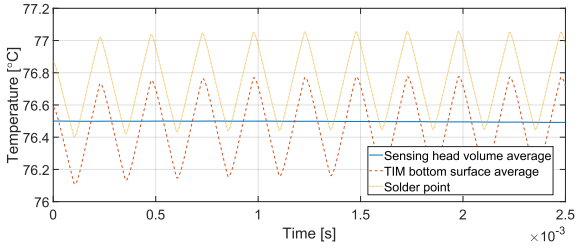

Fig. 9 Point temperature at 4kHz 50A for different layers surfaces

4 Sensor interference analysis

A FBG sensor is an optical fibre sensitive to temperature and mechanical strain variations [7, 8]. A typical single mode optical fibre consists of three layers: core, cladding, and coating [7]. A further detailed discussion of this device is beyond the scope of this paper, thus only characteristics that may be relevant to the sensor installation are further discussed below.

The fibre cylindrical glass core typically has a diameter in the 4-9 µm range. The cladding and coating typical diameters are around 125 µm and 150 µm, respectively and are commonly made of silica glass. On the other hand, the coating is made of polyimide, to offer physical protection to the fibre. In this research assessment, the fibre and TIM are placed above the hot region identified in the previous section (see Fig. 8). To simulate the FBG sensor installation and assess its influence on the local thermal environment, a 125µm diameter [7], cylindrical structure is used to emulate the sensing fibre. For simplicity, a homogeneous material (silica glass) is considered as the fibre material. A box structure, centred on the selected hot spot, and surrounding a section of the fibre, is used to emulate the TIM between the IGBT surface and an assumed 1mm long FBG sensing head. In the simulations the TIM width is assumed to be 4 times the fibre radius, with a length identical to that of the FBG head. The resulting sensing arrangement is shown in Fig. 10. A high thermal conductivity, electrically nonconductive, silicon-based glue is assumed as the TIM in the subsequent studies. The properties of the TIM used in this research are based in a commercially available solution [12] and are listed in Table 3.

For glues, typical minimum bond line thicknesses vary in the range 25-150 µm. Therefore, a conservative 75µm separation between the sensed surface and the bottom of the fibre is assumed in the simulations. Fig. 11 shows simulation results for the temperature measured in the reference point and average temperatures for the sensing head volume and the TIM bottom surface, for IGBT operation at 50A, 4kHz. As can be seen in Fig. 11, the point temperature exhibits a higher peak value. This is expected given the average nature of the other quantities. Furthermore, owing to the considerably lower thermal conductivity of the TIM (compared to the solder layer), the absence of switching detail in the FBG temperature signal was expected to some degree, since the separation between the solder surface and the FBG head is only 75µm; this thickness is considerably greater than that of the IGBT neighbouring layer. Thus, the combination of the TIM relatively low thermal conductivity and relatively large thickness results in a considerably high thermal resistance. Such large thermal resistance restricts the rapid heat transfer process between surfaces during the very fast switching events, and this is reflected in the lack of detail in the sensing head temperature profile.

Fig. 12, compares the temperature of the reference point for pre and post sensor installation scenarios. As shown in Fig. 12, the sensor installation produces a small drop in the local temperature. This behaviour was expected, since the TIM channels the heat away from the sensed surface, acting as a 'cooling tower', producing a local 'cold spot'. However, for the investigated scenario, the thermal disturbance introduced by the sensor is almost negligible and similar thermal effects would be unavoidable with all direct contact sensing techniques. To further assess the effect of the TIM thermal conductivity on the local temperature, TIMs with different thermal conductivities were considered. The obtained results are shown in Fig. 13. It should be noted that only electrically conductive, metal filled glues were found to possess the thermal conductivities matching those shown in Fig. 13. For each increase in TIM thermal conductivity, a further decrease in peak temperature is observed in Fig. 13. However, the temperature decrement is very small. For the cases analysed it is observed to be less than 0.2 °C with respect to the pre-installation reference temperature. Thus, the expected thermal disturbance introduced by sensor installation can be considered negligible, for the analysed cases. Similar results were obtained for different switching frequencies and load currents, these results are omitted here for brevity. Thus, it can be concluded that direct installation of FBG thermal sensors on the IGBT chip surface may result in a minute perturbation of the monitored thermal environment. In practical terms however, such a disturbance can be considered negligible. Another factor that may impact the thermal footprint of the TIM/sensor arrangement is the TIM volume: a higher TIM volume implies that for a given specific heat capacity, more thermal energy can be stored in the TIM.

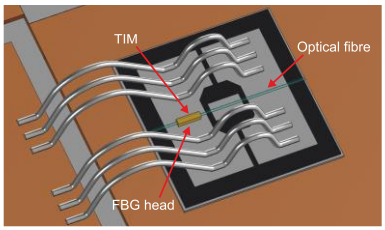

Fig. 10 FBG instrumented IGBT module FE model geometry

Table 3 TIM physical properties

Thermal conductivity [W/m·K]	Heat capacity [J/(kg·K)]	Density [kg/m^3]	Electrical conductivity [S/m]	Dielectric strength [kV/mm]
3.5	1050	3100	-	20

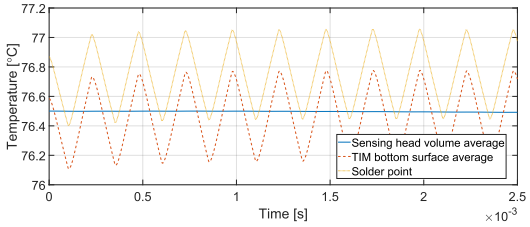

Fig. 11 Post installation temperatures signals

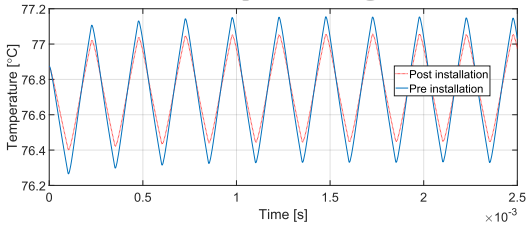

Fig. 12 Pre and post installation point temperature comparison at 4kHz 50A

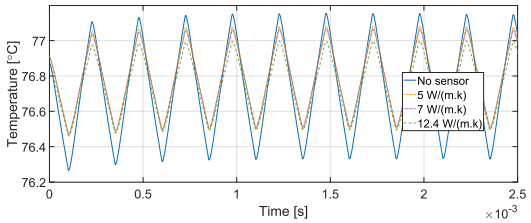

Fig. 13 Point temperature comparison for TIMs with different thermal conductivities at 4kHz 50A

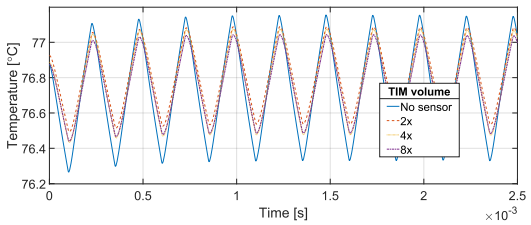

Fig. 14 Pre and post installation point temperature comparison at 4kHz 50A for different TIM volumes

The TIM volume considered in the previous simulations was deliberately chosen to only cover the assumed 1mm long sensing head. However, in practice a larger volume may be required to ensure the sensor effective bond to the surface. To assess the effect that a larger TIM volume may have on the surrounding thermal environment, the volume of the TIM block used in the FE simulations was increased 2, 4 and 8 times its original value. The resulting point temperatures at the reference location are shown in Fig. 14. As can be seen in Fig.14, for each increase in TIM volume a decrease in local temperature occurs. However, even for the highest TIM volume considered, the reduction in temperature is marginal, just about 0.2°C in the worst case. Thus, like with the thermal conductivity increase, the thermal disturbance introduced by the increase in TIM volume can be considered negligible.

5 Conclusion

In this paper, a thermo-electrical finite element model of a commercial IGBT module is developed. With the help of the developed model, the hottest region on the IGBT top solder surface for the sensor installation is identified. The TIM required to enable effective heat transfer between the sensed surface and a hypothetical FBG sensor is considered in the assessment. It was found that the TIM thermal conductivity and mass are factors that can affect the local temperature of the localised area where the sensing head is installed. However, while it was found that the sensor installation introduces disturbances in the original IGBT thermal environment, these were quantified to be at negligible level and of no perceivable concern for practical application. While analysis of further relevant sensing effects and practical tests are required for further assessment, the presented results indicate considerable potential of FBGs for direct on-chip thermal monitoring in IGBT modules.

6 Acknowledgements

The support provided by The Electrical Infrastructure Research Hub with the Offshore Renewable Energy Catapult; and the China Scholarship Council (No. 201906280439) are acknowledged by the authors.

7 References

[1] A. Volke and M. Hornkamp, “IGBT Modules: Technologies, Driver and Application”. Munich, Germany: Infineon Technologies, 2012, pp. 1–2.

[2] H. Oh, et al., "Physics-of-Failure, Condition Monitoring, and Prognostics of Insulated Gate Bipolar Transistor Modules: A Review," in IEEE Trans. on Pow. Elec., vol. 30, no. 5, pp. 2413-2426, May 2015.

[3] S. Yang, et al., “Condition Monitoring for Device Reliability in Power Electronic Converters: A Review,” IEEE Trans. on Pow. Elec., vol. 25, no. 11, pp. 2734-3752, Nov. 2010.

[4] A. Abuelnaga, M. Narimani and A. S. Bahman, "A Review on IGBT Module Failure Modes and Lifetime Testing," in IEEE Access, vol. 9, pp. 9643-9663, 2021

[5] A. Hanif, et al., "A Comprehensive Review Toward the State-of-the-Art in Failure and Lifetime Predictions of Power Electronic Devices," in IEEE Trans. on Pow. Elec., vol. 34, no. 5, pp. 4729-4746, May 2019.

[6] Y. Yang, Q. Zhang and P. Zhang, "A Fast IGBT Junction Temperature Estimation Approach Based on ON-State Voltage Drop," in IEEE Trans. on Ind. App., vol. 57, no. 1, pp. 685-693, Jan.-Feb. 2021.

[7] A. Mohammed et al., "Distributed Thermal Monitoring of Wind Turbine Power Electronic Modules Using FBG Sensing Technology," in IEEE Sensors Journal, vol. 20, no. 17, pp. 9886-9894, 1 Sept.1, 2020.

[8] J. P. Bazzo, et al., 'Thermal characteristics analysis of an IGBT using a Fiber Bragg Grating', Opt. Laser Eng., vol. 50, no. 2, pp. 99-103, 2012.

[9] Q. Huang et al., "A Finite Element Analysis on the Reliability of Heavy Bonding Wire for High-Power IGBT Module," in IEEE Trans. on Comp., Packaging and Manufacturing Tech., vol. 11, no. 2, pp. 212-221, Feb. 2021.

[10] M. Jiang et al., "Finite Element Modeling of IGBT Modules to Explore the Correlation between Electric Parameters and Damage in Bond Wires," 2019 IEEE En. Conv. Congress and Exposition (ECCE), 2019, pp. 839-844.

[11] A. S. Bahman, K. Ma and F. Blaabjerg, "A Lumped Thermal Model Including Thermal Coupling and Thermal Boundary Conditions for High-Power IGBT Modules," in IEEE Trans. on Pow. Elec., vol. 33, no. 3, pp. 2518-2530, March 2018.

[12] SilCool TIA350R Adhesive, available at https://www.silicone-solutions.co.uk/wp-content/uploads/2019/02/TIA350R-Momentive-Technical-Data-Sheet.pdf, last visited 14/10/2021.